HHS Public Access

Author manuscript

*Nat Neurosci*. Author manuscript; available in PMC 2017 March 12.

Published in final edited form as:

*Nat Neurosci*. 2016 December ; 19(12): 1707–1717. doi:10.1038/nn.4386.

# Global dynamics of selective attention and its lapses in primary auditory cortex

**Peter Lakatos**[1,2,*], **Annamaria Barczak**[1], **Samuel A Neymotin**[3,4], **Tammy McGinnis**[1], **Deborah Ross**[1], **Daniel C. Javitt**[1,5], and **Monica Noelle O'Connell**[1]

[1]Cognitive Neuroscience and Schizophrenia Program, Nathan Kline Institute, Orangeburg, NY, USA

[2]Department of Psychiatry, New York University School of Medicine, NY, USA

[3]Department Physiology & Pharmacology, SUNY Downstate Med. Center, Brooklyn, NY, USA

[4]Dept. Neuroscience, Yale University School of Medicine, New Haven, CT, USA

[5]Department of Psychiatry, Columbia University College of Physicians and Surgeons, NY, USA

## Abstract

Previous research demonstrated that while selectively attending to relevant aspects of the external world, the brain extracts pertinent information by aligning its neuronal oscillations to key time points of stimuli or their sampling by sensory organs. This alignment mechanism is termed oscillatory entrainment. We investigated the global, long-timescale dynamics of this mechanism in the primary auditory cortex of nonhuman primates, and hypothesized that lapses of entrainment would correspond to lapses of attention. By examining electrophysiological and behavioral measures we observed that besides the lack of entrainment by external stimuli, attentional lapses were characterized by high amplitude alpha oscillations, with alpha frequency structuring of neuronal ensemble and single unit operations. Strikingly, entrainment and alpha oscillation dominated periods were strongly anti-correlated and fluctuated rhythmically at an ultra-slow rate. Our results indicate that these two distinct brain states represent externally versus internally oriented computational resources engaged by large-scale task-positive and task-negative functional networks.

---

One of the most prominent features of the brain is that it is never in a steady state, its operations perpetually fluctuate on multiple spatial and temporal scales. Often, these fluctuations are temporally regular, spectrally confined, and can therefore be called oscillations. The most common types of neuronal oscillations occur on relatively small, sub-second timescales, and reflect synchronous membrane potential fluctuations of a neuronal ensemble between depolarized and hyperpolarized sates, which maintains ideal excitability[1].

---



Correspondence should be addressed to P.L. (plakatos@nki.rfmh.org).

**AUTHOR CONTRIBUTIONS**: P.L. and M.N.O. designed the study. M.N.O., T.M. and D.R. performed the experiments. P.L. designed the analyses. P.L., M.N.O., A.B. and S.A.N. performed the analyses. P.L. wrote the manuscript with input from all authors.

**COMPETING FINANCIAL INTERESTS**: The authors declare no competing financial interests.

Besides this thermostat like function, the brain also evolved to make use of its neuronal oscillations in a number of other ways, including temporal coordination of neuronal operations via dynamic functional connectivity[2,3], phase-coding of spatial aspects of the environment[4,5], and attentional selection[6–8]. While the sub-second timescale neuronal oscillations instrumenting these brain operations have been extensively studied and we have a reasonable amount of information on their dynamics and functional significance[1], the neuronal underpinnings of long timescale fluctuations of brain states are not known, even though they are evident in neuroimaging studies[9–11], electrophysiological data[12–15], and human behavioral measures[16–18].

In the present study, our main goal was to define global, long-timescale fluctuations of the neuronal dynamics underlying attention and its lapses in auditory cortex. We explored these multi-second dynamics during the performance of a selective intermodal attention task in the primary auditory cortex (A1) of non-human primates. Since the entrainment of neuronal oscillations by attended stimulus streams is well characterized in artificial and natural selective attention conditions, especially in primary sensory cortices[7,19–21], we hypothesized that we could use entrainment as an electrophysiological marker of attention and its fluctuations, allowing us to compare neuronal dynamics during precisely demarcated periods of selective attention and its lapses. To achieve this, we estimated the strength of entrainment in short duration sliding timeframes throughout the performance of a continuous selective attention task. Using behavioral measures, we first verified that periods of entrainment versus a lack of entrainment correspond to periods of selective attention versus attentional lapses, respectively. Next we compared neuronal ensemble dynamics during these two distinct brain states, and found that attentional lapses, besides a lack of oscillatory entrainment by external stimuli, were also characterized by increased alpha frequency band oscillatory activity across all cortical layers. Importantly, we found that entrainment dominated vs. alpha dominated brain states fluctuated rhythmically in counterphase at a rate of approximately 0.06 Hz, independent of task structure, indicating that an internal mechanism is responsible for orchestrating global, long-timescale attentional dynamics. The analysis of neuronal ensemble and single neuron dynamics during entrainment vs. alpha oscillation governed brain states revealed strikingly different patterns of cross frequency coupling, single neuron activity, and interlaminar coherence, likely supporting distinct externally vs. internally oriented, or “task positive” vs. “task negative” brain operations.

## RESULTS

For the present study, we analyzed neuroelectric data recorded in 36 A1 sites of 2 macaque monkeys (20 sites in subject KI and 16 in subject AB). Neuronal activity was recorded with linear array multielectrodes, which spanned all cortical layers. In all experiments, data were obtained via simultaneous left and right hemisphere A1 recordings targeting regions tuned to similar frequencies. To minimize the effects of volume conduction, and attempt to define local transmembrane currents, we calculated one dimensional current source density (CSD) from the field potentials[22] and carried out our analyses on the CSD signals and multi- and single unit activity (MUA and SUA respectively).

During recordings, subjects performed a selective intermodal attention task (Fig. 1a). In separate blocks, the monkeys either had to attend to a rhythmic stream of auditory tone beeps and detect deviant tones (targets) that differed in their frequency, while ignoring the simultaneously presented visual stimulus stream, or vice versa: they had to attend to rhythmically presented LED light flashes and detect deviant flashes (targets) that differed from standards either in color or intensity, while ignoring auditory stimuli. Subjects were instructed to attend to a given modality with the use of a cueing block that preceded selective attention trial blocks and consisted only of the to be attended to modality stimuli. During the presentation of the selective attention trial blocks (lasting 187–239 seconds and containing 32 – 46 targets) 80% of targets were paired with a juice reward, which subjects could collect by sticking out their tongue. On 20% of targets, the juice reward was randomly omitted. These trials were used to monitor performance: a hit was detected if the subjects licked on the juiceless targets, while false alarm was defined as a behavioral response to deviants of the to be ignored modality. Hit and false alarm rates of the two subjects were significantly different in both attend auditory and attend visual trial blocks (Fig 1b), indicating that cueing had a strong effect on behavior.

## Ensemble oscillatory characteristics of attention and its lapses

As we outlined in the Introduction, the first goal of our study was to generate a time-resolved measure for the strength of entrainment, to determine whether it can be used to index attention. To do this, we first determined the cortical layers for each of our recording sites using CSD response profiles related to best frequency (BF) tones (Fig. 2a) and selected the supragranular channel with the largest amplitude sink (red blob in color map) for inter-trial coherence (ITC) analyses, since previous studies pinpoint this laminar location as the site of strongest oscillatory entrainment[7,20,23]. Albeit BF tone related CSD profiles were used to determine laminar electrode locations, for our further analyses we selected artifact free recordings during which non-best frequency (non-BF) tones constituted the auditory stream, with frequencies at least 2 octaves different from the BF of the recording site (Fig. 2a inset). The reason for this is that responses to non-BF tones are subthreshold in nature, without significant stimulus related MUA or CSD amplitude increases (evoked response), that could distort phase/ITC estimates[20,24], which are used to index entrainment. Next, we extracted the phases of the supragranular delta oscillation that corresponded to the repetition rate of stimuli (auditory = 1.6 and visual = 1.8 Hz) at stimulus onset in 5 second windows and calculated ITC (Fig. 2b). The step size of the moving window was 1 second (resulting in a 1 Hz “sampling rate”). Significant ITC values related to either modality stimuli indicate that delta oscillations in a given time window are “locked” to or entrained by the stimuli, while non-significant ITC values signal that the phase of oscillations is random at the time stimuli are presented due to a lack of oscillatory entrainment (Fig. 2b).

As Figure 3a illustrates, the moving ITC measure fluctuates strongly, both when calculated for auditory (green trace) and for simultaneously presented visual stimuli (purple trace), independent of whether the monkey is cued to attend to auditory (upper) or to visual stimuli (lower). Based on the significance of auditory and visual related moving ITC, four “entrainment categories” can be distinguished: 1) significant auditory stimulus related delta ITC (ITCa) indicating auditory entrainment, 2) significant visual stimulus related delta ITC

(ITCv) signaling visual entrainment, 3) no significant ITC (noITC) and 4) significant ITC related to both streams (ITC both). As the boxplots in Figure 3b demonstrate, similar to behavior, cueing also had a significant effect on entrainment. In attend auditory trial blocks, auditory ITC periods occur significantly more often than any other entrainment categories, and likewise visual ITC dominates in attend visual trial blocks. The occurrence of periods marked by entrainment to the to be ignored (or un-cued) modality and no-entrainment did not differ significantly. Periods in which both auditory and visual ITC were significant (ITC both) occurred significantly less than any other entrainment category, and sometimes not at all in a trial block (Fig. 3a–b). In line with previous studies[20,23], these results indicate that, at least in A1, entrainment is exclusive: only one stimulus stream entrains oscillations at any given time. Therefore, we excluded rare time-windows when ITC was significant for both stimulus streams from further analyses.

To verify our initial hypothesis that oscillatory entrainment – measured as significant ITC – can be used as an indicator of selective attention, we examined the distribution of hits and false alarms during the different entrainment categories. As the bar plots in Figure 3b illustrate, nearly all hits occurred during periods of entrainment to the cued modality (82.9% in attend auditory and 83.4% in attend visual trial blocks), while nearly all false alarms occurred during periods of entrainment to the un-cued modality (87.1% in attend auditory and 76.1% in attend visual trial blocks). This indicates that the “modality of entrainment” is indeed a good indicator for the modality the subjects are selectively attending to. Both entrainment and behavioral measures indicate that while cueing successfully biased the monkey’s attention towards the desired modality stimuli, at times, the subjects were switching their attention to the un-cued (to be ignored) modality. During periods of no entrainment, the monkeys had significantly less hits compared to entrainment to the cued, and significantly less false alarms compared to entrainment to the un-cued modality streams(Fig. 3b bar plots), indicative of attentional lapses.

Taken together, these results provide solid support for our hypothesis that oscillatory entrainment can be used to index the modality and strength of selective attention, and that differing entrainment patterns outline distinct brain states: one indicative of selective attention to the auditory stream (ITCa), one of selective attention to the visual stream (ITCv), and a third state of attentional lapse (noITC). In an attempt to reveal mechanistic information, we investigated how neuronal oscillatory dynamics differ across these three attentional states. We started by comparing supragranular auditory stimulus related ITC, and power spectra averaged across all layers (Fig. 3c). As expected, and as the upper row of time frequency and p-value plots in Figure 3c illustrate, auditory stimulus related ITC is greater at certain frequencies during auditory entrainment, independent of cueing context. One of these frequencies is delta, since significant delta ITC was used to define auditory entrainment. Other frequencies correspond to theta and gamma oscillations, which have been shown to be dominant in the spectrum of ongoing supragranular neuronal ensemble activity[24]. This is also not surprising since the phase reset of ongoing oscillations, indexed by ITC, is a prerequisite for entrainment, and prior studies have found that phase reset in the theta and gamma frequency bands accompanies delta reset and entrainment[24]. A two-way ANOVA carried out on ITC values averaged within the different frequency bands in the 20–100 ms post-stimulus time-frame verified these findings: while the effect of entrainment (ITCa,

ITCv or no-ITC) was significant for delta ($F(2,210)=146.95$, $p=1.22\times10^{-40}$), theta ($F(2,210)=3.95$, $p=0.02$) and gamma oscillations ($F(2,210)=5.18$, $p=0.006$), the effect of cueing (attend auditory vs. attend visual) was not significant in any of the frequency bands ($F_{delta}(1,210)=0.47$, $p_{delta}=0.49$; $F_{theta}(1,210)=1.49$, $p_{theta}=0.22$; ; $F_{alpha}(1,210)=0.47$, $p_{alpha}=0.49$; $F_{beta}(1,210)=0.34$, $p_{beta}=0.56$; $F_{gamma}(1,210)=3.13$, $p_{gamma}=0.07$). There was no interaction of entrainment and cueing ($F_{delta}(2,210)=0.1$, $p_{delta}=0.90$; $F_{theta}(2,210)=0.69$, $p_{theta}=0.5$; $F_{alpha}(2,210)=0.1$, $p_{alpha}=0.9$; $F_{beta}(2,210)=0.06$, $p_{beta}=0.93$; $F_{gamma}(2,210)=0.04$, $p_{gamma}=0.96$). These results verify and extend previous observations that selective attention to a given modality is indexed by the phase reset of oscillations in the delta, theta and gamma frequency bands, while ignoring stimuli (attention to a different modality) and attentional lapses are both characterized by a lack of phase reset.

Next, we compared oscillatory amplitudes and found that similar to ITC, cueing had no effect (two-way ANOVA, $F_{delta}(1,210)=0.22$, $p_{delta}=0.63$; $F_{theta}(1,210)=0.13$, $p_{theta}=0.71$; $F_{alpha}(1,210)=0.02$, $p_{alpha}=0.88$; $F_{beta}(1,210)=0.0008$, $p_{beta}=0.97$; $F_{gamma}(1,210)=0.01$, $p_{gamma}=0.9$). These results suggest that the quality of the three distinct attentional states does not differ in the 2 different cueing contexts, cueing merely increases the length of one of these – attention to the cued modality stimuli (see above). As opposed to the effect of cueing, comparing amplitude values across the different frequency bands revealed that entrainment had a significant effect on amplitudes in the alpha, beta and gamma frequency bands ($F_{alpha}(2,210)=20.86$, $p_{alpha}= 6.6\times^{-08}$; Fbeta$(2,210)=10.95$, $p_{beta}=1.2\times10^{-04}$; $F_{gamma}(2,210)=11.73$, $p_{gamma}=2.7\times10^{-05}$). As the lower row of time frequency and p-value plots in Figure 3c illustrates, in contrast to ITC measures, there appear to be no amplitude differences between auditory (ITCa) vs. visual entrainment conditions (ITCv). Rather, alpha, beta and gamma amplitudes are greater during periods that lack entrainment (noITC). To estimate the laminar location of these amplitude differences, we aligned laminar spectral amplitude profiles across all experiments (see methods) and statistically compared amplitude differences during entrainment vs. no-entrainment periods (Fig. 3d). Since we found no effect of cueing on any spectral measures across the three different entrainment conditions (as described above), we merged the data recorded in attend auditory and attend visual trial blocks. We found that increased alpha-beta-gamma amplitudes during no entrainment time periods were widespread across the different cortical layers. Our layer specific amplitude maps also revealed an opposite sign change in delta amplitude at the frequency of auditory (ITCa vs. noITC) and visual stimulus repetition rate (ITCv vs. noITC), but only in the supragranular layers (Fig. 3d). This latter finding in the supragranular layers can be explained by the presence of greater delta energy at the frequency of entrainment[20], therefore, in the following we will only focus on the alpha-beta-gamma effect.

## Slow counterphase oscillatory dynamics

Our results thus far show that alpha amplitude across all cortical layers is increased during periods that lack entrainment to stimulus streams. Therefore, it is not surprising that by overlaying moving delta ITC and alpha amplitude, we find an opposite sign modulation (Fig. 4a): whenever delta ITC is high, alpha amplitude is low and vice versa. What is surprising is that this counter-sign modulation appears to be rather rhythmic throughout the entire trial block, and that it seems slower than the rhythm of the task (defined as the average frequency

of target stimulus occurrence (0.16 Hz). To quantify these observations, we first calculated the spectra of moving delta ITC and alpha waveforms. As the examples in Figure 4b illustrate, both ITC and alpha spectra exhibit prominent peaks around 0.06 Hz, and the ITC spectra display a second peak around 0.15 Hz. This second peak was often absent from the moving alpha amplitude spectra. As the boxplots of the pooled data show (Fig. 4c), the prominent lower frequency peaks in moving ITC and alpha amplitude spectra were not significantly different from each other when pooled across all experiments (n=36, Wilcoxon signed rank, p=0.19), but both were significantly different from the task frequency ( n=36, Wilcoxon signed rank, $p_{ITC}=3.64\times10^{-07}$, $p_{alpha}=3.99\times10^{-07}$ ). The higher frequency peak detectable in the delta ITC spectrum was, on the other hand, not significantly different from the task frequency (n=36, Wilcoxon signed rank, p=0.072). These results indicate that the most prominent fluctuation of attention, indexed by opposing modulation of entrainment and alpha amplitude, is independent of the task structure.

To determine whether the time-courses of moving ITC and alpha amplitude waveforms are anti-correlated as their opposite sign modulation suggests, we measured the amount of bias in the distribution of their phase differences (coherence) at the frequency of the dominant peak in the alpha amplitude spectrum. We found significant coherence (Rayleigh $p<0.05$) of moving ITC and moving alpha amplitude waveforms in 33 out of 36 experiments. As the histogram in Figure 4d shows, mean phase differences (ITC vs. alpha) are significantly biased towards a half oscillatory cycle, which verifies the anti-correlated delta ITC–alpha amplitude relationship.

To test whether moving ITC and alpha reflect local or more global long timescale fluctuations of neuronal dynamics, we calculated the coherence of moving ITC and alpha amplitude waveforms in simultaneous left and right hemisphere recordings (Fig. 4e). We found that all but one paired recordings displayed coherent (Rayleigh $p<0.05$) inter-hemispheric delta ITC and alpha amplitude fluctuations, with mean phase difference distributions significantly biased towards zero. This signals that both delta ITC and alpha amplitude are modulated synchronously across hemispheres, indicative of the involvement of large scale networks rather than local neuronal ensemble mechanisms in the orchestration of anti-correlated entrainment–alpha amplitude fluctuation.

## Distinct delta-theta versus alpha-beta referenced operational modes

As Figure 3c shows, besides alpha, the amplitude of beta and gamma oscillations also increased during periods of attentional lapses, when delta oscillations were not entrained by any of the sensory stimulus streams. The observation of increased beta amplitudes during no-entrainment periods characterized by high amplitude alpha oscillatory activity is in line with previous findings indicating that alpha and beta oscillations are co-modulated in time and co-localized in space[25–28], therefore seemingly supporting similar neuronal operations. However, the finding that gamma amplitude is also higher during periods characterized by increased alpha is surprising, since alpha is usually associated with suppression and gamma is typically an indicator of excitability. Hence, high alpha amplitudes should result in suppressed gamma frequency band neuronal activity, which is what prior studies have found[29–31]. This discrepancy led us to further investigate the gamma amplitude enhancement

that occurs during no-entrainment time periods. Since it is well documented that, rather than being continuous, gamma band neuronal activity occurs in bursts[30], we decided to examine the properties of gamma bursting during entrainment (significant ITC) vs. no-entrainment (non-significant ITC) periods (Fig. 5). We first tested the peak frequency of gamma bursts in distinct cortical layers, and found no effect of entrainment across trial blocks (n=72, Wilcoxon signed rank, $p_{supragranular}$=0.6, $p_{granular}$=0.38, $p_{infragranular}$=0.93). In contrast, we found a significant increase in the amplitude of gamma bursts during no-entrainment time periods in the granular layer (Fig. 5b). Additionally, we found that the rate at which gamma bursts occurred was significantly increased across all layers during no-entrainment time periods (Fig. 5c), which – together with the burst amplitude increase in the granular layer – could account for the gamma amplitude increase observed in the averaged laminar profiles (Fig. 3d).

The distinction between the amplitude and rate of gamma bursting is important since the gamma amplitude differences observed in the time-averaged data (Fig. 3d) do not have to be directly related to changes in gamma amplitude per se, but rather could be due to the re-structuring of gamma bursts. Therefore, we examined whether increased gamma rates could be associated with changes in cross frequency coupling by measuring how the timing of gamma bursts correlates with the phase of neuronal ensemble activity at lower frequencies. Figure 5d shows averaged burst-CSD coherence spectra from the supragranular, granular and infragranular layers. Higher values indicate stronger gamma-burst – CSD coupling at a given frequency. We found stunning opposite sign differences in gamma burst–theta phase and gamma burst–alpha phase coupling. While during periods of entrainment, theta-gamma and to a lesser degree delta-gamma phase-amplitude coupling dominate, especially in the supragranular layers, during no-entrainment periods alpha-gamma coupling takes over in all cortical layers. Thus, phase amplitude coupling undergoes radical changes during switches between delta entrainment and high alpha dominated brain states.

Since gamma frequency neuronal activity and multiunit activity usually display correlated amplitude changes, we tested whether, similar to gamma, MUA is also increased during no-entrainment time periods. We found that indeed, MUA of all cortical layers was significantly greater during no-entrainment periods (n=72, Wilcoxon signed rank, $p_{supragranular}$=0.0264, $p_{granular}$=0.0043, $p_{infragranular}$=0.0019), which is again a counterintuitive finding in light of the commonly accepted suppressive role of alpha oscillatory activity. Therefore, we decided to further dissect the MUA amplitude effect by characterizing single unit firing properties during entrainment and no-entrainment periods.

Altogether, 1167 single units were isolated from the 36 A1 multielectrode recordings. Below the averaged spike waveform in Figure 6a, the histogram shows the distribution of spike durations as defined by peak-to-trough time, with three obvious peaks. Based on previous studies examining the detailed differences in spike waveform and spike train statistics[32–35], the long and medium duration waveforms likely correspond predominantly to the spiking of putative excitatory neurons and inhibitory neurons respectively. While short duration waveforms (SDWs) are not often isolated, a recent study suggests that these might reflect afferent spiking activity[35].We arbitrarily assigned parts of the distribution to these categories, acknowledging that there is likely considerable overlap between the groups with

different spike durations. Nevertheless, in line with the literature, median spike rates were significantly higher in the putative inhibitory neuron group compared to both other groups ($n_{inhibitory}$=589, $n_{excitatory}$=490, $n_{SDW}$=88, Wilcoxon rank sum, $p_{inhibitory\text{-}excitatory}=2.33\times10^{-4}$, $p_{inhibitory\text{-}SDW}= 4.09\times10^{-11}$). Figure 6b shows firing rates during entrainment (significant ITC) versus no-entrainment (non-significant ITC) periods for all neurons, and separately for the different putative cell types. We found that all neuronal groups displayed significantly increased firing rates during no-entrainment periods. This corroborates our MUA result and raises the question: similar to the case of gamma bursts, do increased firing rates reflect distinct spike-CSD coherence patterns? The pooled data displayed in Figure 6c indicates that this is indeed the case. If we consider all neurons, delta-theta spike-CSD coherence is greater during entrainment, while alpha-beta spike-CSD coherence dominates no-entrainment periods. Whereas across different brain states delta-theta-alpha effects dominate in putative excitatory neurons, alpha-beta spike-CSD coherence changes dominate in putative inhibitory interneurons. We found neither distinct spike-CSD coherence patterns nor any entrainment related changes in the case of SDWs. These results indicate that in general, the firing of A1 neurons is structured dominantly by delta-theta oscillatory activity during selective attention to rhythmic external stimuli, and to alpha-beta oscillatory activity during lapses of attention.

The repetitive combination technique used when calculating spike-CSD coherences enabled us to detect significant differences of spike-CSD coherence between entrainment and no-entrainment periods for every single unit (see Methods). We found that 24% of all units displayed a significant delta-theta spike CSD coherence increase during entrainment, 25% displayed a significant alpha-beta spike CSD coherence increase during no-entrainment periods, and 9% displayed both (Fig. 6d). If spike-CSD coherence indicates how strongly a given neuron is integrated in synchronous neuronal ensemble operations orchestrated by neuronal oscillations, this result might mean that while certain neurons are recruited during attentive brain states, others are utilized more during attentional lapses, with a proportion being able to switch between operational modes.

Besides calculating “local” spike-CSD coherences, we can also calculate the laminar spike-CSD profile of any single neuron, as shown in Figure 6e. These profiles reveal strikingly different coherence patterns during entrainment (top) vs. no-entrainment (bottom) periods, and not just in frequency, but also in cortical space. Therefore, we decided to investigate the laminar coherence patterns that characterize entrainment vs. no-entrainment brain states, since these likely reflect differing functional connectivity patterns that funnel the effect of neuronal spiking towards differing neuronal computations.

Figure 7a shows representative laminar coherence matrices displaying delta (on top) and alpha (on bottom) CSD coherence across all electrode pairs during periods of entrainment (significant ITC, left) vs. no-entrainment (non-significant ITC, right). It is apparent that, while the networks delineated by delta and alpha coherence patterns overlap, they also show distinct characteristics. Delta coherence is strongest within and across supra and infragranular sites, while alpha coherence highlights interconnected nodes within all cortical layers. The differences between entrainment and no-entrainment conditions might not be obvious from the coherence matrices, so we averaged coherence values along one spatial

dimension, creating a one-dimensional laminar coherence index (traces to the right of the coherence matrices in Fig. 7a). This index describes for each recording location (y axis), how strongly neuronal activity is coherent with neuronal activity at all other locations (x-axis). As the representative example in Fig. 7a shows, there are significant counter-sign differences in delta and alpha cross-laminar coherence between entrainment and no-entrainment brain states. While supragranular and infragranular delta coherence is increased during entrainment, alpha coherence across all layers is increased during no-entrainment periods. Interestingly, while in the majority of individual laminar coherence profiles, like in Figure 7a, delta coherence differences were not significant in the granular layer, the difference was significant in the pooled data (Fig. 7b). To summarize, while interlaminar functional delta coherence is stronger during attention to rhythmic stimulus streams, alpha coherence across cortical layers is stronger during lapses of attention, emphasizing differing interlaminar connectivity patterns specific to delta and alpha oscillations respectively, resulting in the distinct routing of information.

## DISCUSSION

Our current study revealed that the entrainment of neuronal oscillations supporting the selection and attentive processing of rhythmic stimulus streams[7,19–21] is far from stable during the performance of a continuous selective attention task. There are lapses of entrainment occurring at regular, 10–30 s time intervals, that correspond to lapses of attention and behavioral responding. While periods of oscillatory entrainment are characterized by delta-theta frequency patterning of gamma oscillatory activity (Fig. 5d) and neuronal firing (Fig. 6c), lapses of entrainment are characterized by the increased amplitude of alpha oscillations, and alpha frequency band patterning of high frequency neuronal ensemble (Fig. 5d) and single neuron activity (Fig 6c). Together with divergent variations in interlaminar cortical coherence between entrainment and no-entrainment brain states (Fig. 7), these data outline two distinct operational modes of auditory cortical neuronal populations, that likely subserve distinct perceptual-cognitive functions. The counter-phase fluctuation of neuronal dynamics we detected in primary auditory cortex bares striking similarities to the counterphase fluctuation of resting state oscillations detected by neuroimaging studies[10] and their correlation to alpha-beta frequency band EEG activity in humans[36,37]. We therefore propose that the distinct neuronal ensemble and single neuron dynamics described by our study reflect the linking of auditory cortex machinery to task positive (entrainment) vs. task negative (high alpha) large scale functional networks.

One of the most important findings of our current study is that the slow counterphase modulation of entrainment vs. no-entrainment periods is independent of the temporal structure of the task (Fig. 4c). This indicates that the slow fluctuations of neuronal dynamics observed in our study are orchestrated by internally timed mechanisms, which is why we argue that it can be linked to large scale functional networks detected in neuroimaging studies[9–11]. While anti-correlations in the fMRI signal have been proposed to be simply an artifactual consequence of global-signal regression[38], our electrophysiological findings provide confirmation that counterphase modulations of the patterning of neuronal activity do occur in cortical neuronal ensembles on temporal scales that are comparable to the low-frequency fluctuations identified by neuroimaging studies. Alternatively, as a recent study by

van den Brink et al.[39] demonstrated, periods of "no entrainment" observed in our data could occur following behavioral errors. However, since the overall false alarm rate was low in our study (Fig 1b), and in some trial blocks false alarms did not occur at all, (Fig 3b), this explanation is unlikely. Nevertheless, the second, higher frequency peak in the moving ITC spectrum, which corresponds to the rate at which targets occurred (ITC2, Fig. 4b–c), might be due to a similar process that distracts from the current task and diminishes entrainment temporarily following target stimuli.

Despite our subjects' poor behavioral performance during the no-entrainment, high alpha amplitude periods, our data challenge the notion that alpha oscillations merely reflect suppression, if, as customary, gamma oscillatory amplitudes and neuronal firing rates are taken as indicators of neuronal ensemble excitability, since we found that both of these increased during the high alpha amplitude brain state. This seems to indicate that in addition to controlling excitability, the main role of neuronal oscillations – including alpha – is to impose differing activity patterns on neuronal ensembles, a side effect of which might be impaired responding to stimuli. These contrasting activity patterns in turn likely promote distinct brain operations, like active sensing vs. internal information processing, and corresponding bottom up vs. top-down dominated information flow. Interestingly, Haegens and colleagues also found an overall firing rate increase during highest alpha amplitude periods in primary somatosensory cortex, but not in secondary somatosensory, or motor cortices[40], indicating that primary cortices might differ in alpha related effects from other regions. Alternatively, since we have overwhelming evidence that the brain does utilize alpha oscillations to suppress cortical regions that are irrelevant for goal directed sensory processing (for a review see[41]), it is possible that this most commonly detected "suppressive alpha" is different from the "timing alpha" described by our study and the study of Saalmann and colleagues[42]. We speculate that the only reason functionally different alpha rhythms occupy the same frequency space is that they are both referenced to internal timing mechanisms (pacemaker neurons or microcircuits), and not to external stimuli or the pattern of their sampling like delta-theta oscillations. Womelsdorf and colleagues[43] also suggested that there are at least two different types of alpha rhythms in sensory cortices: an infragranularly initiated suppressive alpha, and a pulvinar initiated alpha that is meant to enhance relevant information. They speculate that the cortical signature of this latter alpha operational mode should be widespread alpha–gamma cross frequency coupling involving all cortical layers, which is what our study found during periods when delta rhythms were not entrained by sensory stimuli. Our data provide strong support for the hypothesis that different brain states are characterized by distinct dynamic motifs[43], that likely support differing effective connectivity patterns and thereby neuronal computations subserving the selection and integration of relevant information.

The finding that different neurons preferentially synchronize their firing to local neuronal ensemble oscillations either during entrainment or during periods dominated by alpha oscillations indicates that by changing the frequency of its neuronal ensemble oscillations, the brain might be able to engage distinct neuronal populations. We found that while there are neurons that preferentially fire on certain phases of local delta-theta neuronal ensemble oscillations during entrainment, others synchronize their firing to neuronal ensemble oscillations only during high alpha operational modes (Fig. 6d). This is likely due to the

different neurons' or neuronal ensembles' resonance properties determined by their cellular properties and/or connectivity patterns[43,44]. A relatively small portion (9%) of neurons we detected could synchronize their firing both to delta-theta and alpha-beta neuronal ensemble oscillations, possibly due to their less sharply tuned cellular-network resonance properties. We hypothesize that when neurons do not synchronize their firing to synchronous neuronal ensemble rhythms, the effect of their firing is diminished and they are excluded from neuronal computations due to the lack of "functional convergence" on their target neurons. Thus, even though they fire at the same or even higher rate during different brain states, their action potentials will not be taken into account for the currently relevant brain operation. While future modeling and single cell studies are needed to verify this scenario, our data provide strong support for the notion that by simply switching the frequency at which cortical neuronal ensembles oscillate, distinct neuronal groups can be recruited and effectively connected by distinct intra- and interlaminar oscillatory patterns.

In the introduction we attributed short timescale oscillations in neuronal ensembles as a means for maintaining an ideal excitability state while conserving energy[1]. Along this line of thought, what might the long timescale variations of neuronal ensemble dynamics uncovered by our study and numerous prior studies be meant to maintain? Based on our current results we propose that they maintain an ideal balance of delta-theta entrainment dominated external vs. alpha-beta dominated internal oriented information processing. If true, ultra-slow resting state oscillations maintaining this perceptual-cognitive balance likely exist so that brain operations are not "captured" by the external or the internal environment for long periods of time. For example, the unavoidable "return" of the alpha dominated brain state during selective attention would allow for detaching from external stimulation, reevaluating current goals, and updating the cognitive context in which external stimuli are evaluated. In this theoretical framework, if this "detaching mechanism" overacts, the brain simply cannot connect to the external world, which might be the underlying cause of the lack of entrainment in Schizophrenia[45]. In fact, several recent neuroimaging studies provide evidence that the task negative default mode network is indeed overactive in Schizophrenia patients[46,47], and that this is accompanied by increased alpha frequency band neuronal activity in the same regions[48].

As we previously proposed[49], the two hubs orchestrating externally (entrainment) vs. internally (high alpha) directed information processing dynamics could be core-matrix organized thalamic relay nuclei on one hand and the pulvinar on the other, with the thalamic reticular nucleus balancing their influence in counterphase. While this hypothesis needs to be tested, it is feasible to think that impairments at any node of this large scale thalamocortical system maintaining the perceptual-cognitive balance would lead to psychiatric and neurodevelopmental disorders, like schizophrenia and ADHD. Global dynamics of the moving ITC measure used in our study could provide a useful tool to aid diagnosis in these cases, and since moving ITC enables tracking attention practically in real-time, it could also provide the basis for closed-loop biofeedback therapeutic techniques, or training of attention[50]. In addition, this measure might prove to be an extremely useful tool in assessing attention in subjects who cannot cooperate easily, like infants and autistic subjects.

To summarize, we identified two distinct, counterphase fluctuating brain states in the auditory cortex of subjects performing a selective intermodal attention task. These brain states were characterized by distinct neuronal dynamics: one framed by oscillations adapting to the temporal structure of external events and one by alpha oscillations, providing an external linked versus internal linked temporal reference frame for the coordination of neuronal computations. The slow fluctuation of these two brain states likely reflects the counterphase modulation of task positive and task negative large scale networks, which we propose is meant to maintain an ideal perceptual-cognitive balance.

## ONLINE METHODS

### Subjects

In the present study, we analysed the electrophysiological data recorded during 36 penetrations of area A1 of the auditory cortex in 2 female rhesus macaques (ages 7 and 11, weighing 5–7 kg), who had been prepared surgically for chronic awake recordings. Prior to surgery, each animal was adapted to a custom fitted primate chair and to the recording chamber. All procedures were approved in advance by the Animal Care and Use Committee of the Nathan Kline Institute.

### Surgery

Preparation of subjects for chronic awake intracortical recording was performed using aseptic techniques under general anesthesia. The tissue overlying the calvarium was resected and appropriate portions of the cranium were removed. The neocortex and overlying dura were left intact. To provide access to the brain and to promote an orderly pattern of sampling across the surface of the auditory areas, plastic recording chambers (Crist Instrument Co.) were positioned normal to the cortical surface of the superior temporal plane for orthogonal penetration of area A1, as determined by pre-implant MRI. Together with socketed Plexiglas bars (to permit painless head restraint), they were secured to the skull with orthopedic screws and embedded in dental acrylic. A recovery time of six weeks was allowed before behavioral training and data collection began.

### Electrophysiology

During the experiments, animals were monitored with infrared and/or low light cameras as they sat in a primate chair in a dark, isolated, electrically shielded, sound-attenuated chamber with head fixed in position. Neuroelectric activity was obtained using linear array multi-contact electrodes (23 contacts, 100 μm intercontact spacing, Plexon Inc.). The multielectrodes were inserted acutely through guide tube grid inserts, lowered through the dura into the brain, and positioned such that the electrode channels would span all layers of the cortex (Fig. 2a). Final position was determined by inspecting the laminar response profile to binaural broadband noise bursts. Neuroelectric signals were impedance matched with a pre-amplifier situated on the electrode (10x gain, bandpass dc-10 kHz), and after further amplification (500x) signals were recorded continuously with a 0.1 – 8000 Hz bandpass digitizer with a sampling rate of 20 kHz and precision of 16-bits using custom made software in Labview. The signal was divided into field potential (0.1–300Hz) and MUA (300–5000Hz) range by zero phase shift digital filtering ($2^{nd}$ order Butterworth filter).

MUA data was also rectified in order to improve the estimation of firing of the local neuronal ensemble[51]. One-dimensional current source density (CSD) profiles were calculated from the local field potential profiles using a three-point formula for the calculation of the second spatial derivative of voltage[22,52]. The advantage of CSD profiles is that they are not affected by volume conduction like the local field potentials, and they also provide a more direct index of the location, direction, and density of the net transmembrane current flow[22,52]. At the beginning of each experimental session, after refining the electrode position in the neocortex, we established the best frequency (BF) of the recording site using a "suprathreshold" method[53,54]. The method entails presentation of a stimulus train consisting of 100 pseudorandom order occurrences of a broadband noise burst and pure tone stimuli with frequencies ranging from 353.5 Hz to 32 kHz in half octave steps (duration: 100 ms, r/f time: 5 ms, SOA = 624.5). Auditory stimuli were produced using Tucker Davis Technology's System III coupled with MF-1 free field speakers.

### Behavioral task and stimuli

We trained 2 monkeys to perform an intermodal selective attention oddball task, which required them to attend to and discriminate stimuli in one modality while ignoring stimuli in the other modality (Fig. 1). Auditory and visual stimulus streams were presented simultaneously with differing stimulus onset asynchronies (SOAs) so that visual and auditory stimuli did not have a constant temporal relationship. This was meant to eliminate any multisensory "binding" effects, and facilitate the segregation of the two different modality streams. Monkeys were cued to either detect frequency deviants occurring at random time intervals in the auditory stream, or to detect a color or intensity change in rhythmic LED flashes. The auditory stream consisted of pure tone beeps at 40 dB SPL (25 ms duration, 5 ms rise/fall time) with a constant stimulus onset asynchrony (SOA) of 624.5 ms, equivalent to a 1.6 Hz repetition rate, while the visual stream had a 1.8 Hz repetition rate. The repetition rates were set so that they would correspond to the delta frequency range of ongoing neuronal activity. The frequency of the auditory standards was parametrically varied across blocks in half octave steps between 0.3–32 kHz, resulting in 14 different frequency tone streams. Trial blocks utilizing the different frequency tone streams were presented in random order. Frequency deviants (~ 4 semitones different from the standard) occurred in the stream of standard tones every 3–9 seconds randomly. As described above, during the course of an experiment, monkeys were presented with 14 different frequency tone streams in both "attend auditory" and "attend visual" trial blocks, with the purpose of estimating attention related changes in frequency tuning[23]. In the present study we only analyzed neuronal activity related to one of these streams for each attention condition. To avoid large amplitude event-related responses related to preferred frequency, or best frequency (BF) tones (Fig. 2a), that can influence both spectral phase and amplitude measures, we chose to analyze non-best frequency (non-BF) trial blocks in which the tone frequency was at least 2 octaves different from the best frequency[24]. The reason for this is that although entrainment occurs, responses to non-BF tones are subthreshold in nature, without significant stimulus related MUA or CSD amplitude increases (evoked response), that could distort phase/ITC estimates[20,24]. We verified that there were no evoked responses related to auditory stimuli by statistically comparing the analytic (Hilbert) amplitude of pre- (−150 - −50 ms) and post-stimulus (0 – 100 ms) CSD averaged across all channels

(Wilcoxon signed rank, number of auditory trials = 299–382, all $p>0.05$). Since we wanted to calculate continuous long timescale measures of oscillatory entrainment and dynamics, if movement or behavioral response related artifacts were obvious in the continuous recording or continuous spectrogram, we chose the trial block with the next closest frequency tone devoid of artifacts. We did originally consider including more non-BF trial blocks per experiment, however, we realized that a lot of these had movement artifacts that would have impacted our moving alpha/ITC measures, thus ultimately we decided to limit our analyses to the single "cleanest" recording per attention condition.

Training of subjects on the intermodal selective attention task began with the auditory paradigm, using a single stream of tones. To facilitate the monkey's attention to the rhythmic stimulus streams, at the start of training, 0.25–1 ml juice rewards were delivered simultaneously with each deviant through a spout. The spout was positioned such that the monkeys had to stick out their tongue to get the juice. Licking was monitored using a simple contact detector circuit[55]; the output of which was continuously recorded with Labview together with the timing of standard and deviant tones for offline analyses. In this early phase of training, the frequency difference between the standard and deviant tones was one octave. After 2 sessions, the juice reward was omitted on every $10^{th}$ deviant. If the monkeys licked on the deviants without a paired juice reward, this signaled that they were attending to the tones and actively discriminating the deviants. We then omitted the reward on 20% of the deviants, and gradually lowered the frequency difference to 2–4 semitones. After 10–20 sessions on average, the monkeys' performance became relatively stable: they were reliably licking on juiceless deviants before the next stimulus occurred in the train. At this time, we introduced the visual stream first in isolation, and after 2–3 sessions, when the monkeys reliably responded to visual deviants we started to overlap streams. Finally, we introduced cueing streams, the same stimulus sequences used in the overlapped, intermodal selective attention blocks, but presented in one modality only, to indicate the target modality for attention in the upcoming intermodal selective attention trial block. As determined by licking behavior on juiceless deviants (Fig. 1), one of the subjects performed this task 76% correct while the other monkey performed only 64% correct. Performance remained stable throughout the course of all experiments. Data collection and analysis were not performed blind to the conditions of the experiments. All experiments were performed during the day, between 8 AM and 5 PM.

## Data analysis

Data were analysed offline using native and custom-written functions in Matlab (Mathworks, Natick, MA). After selective averaging of the CSD and MUA responses to the tones presented in the suprathreshold tonotopy paradigm, recording sites were functionally defined as belonging to A1 or belt auditory cortices based on the sharpness of frequency tuning, and the inspection of the tonotopic progression across adjacent sites[53,56,57]. In the present study, only recordings obtained from area A1 were analysed. At the end of each animal's experimental participation, functional assignment of the recording sites was confirmed histologically.

While we utilized the BF-tone related laminar CSD profiles to functionally identify cortical layers in area A1 (Fig. 2a), all further analyses were conducted on recordings during trial blocks consisting of non-BF tones (see above).

Continuous oscillatory amplitudes and phases were extracted by wavelet decomposition (Morlet wavelet, $\sigma = 6$). To characterize phase distributions across trials, the wavelet transformed single trial data were normalized (unit vectors), the trials were averaged, and the length (modulus) of the resulting vector was computed (e.g.[23]). The value of the mean resultant length, also called inter-trial coherence (ITC), ranges from 0 to 1 with higher values indicating that the observations (oscillatory phase at a given time-point across trials) are clustered more closely around the mean than lower values (phase distribution is biased). Significant deviation from uniform (random) phase distribution was tested with Rayleigh's uniformity test.

To obtain an estimate of the strength of entrainment during an entire trial block, we calculated delta ITC at the frequency corresponding to the repetition rate of auditory (1.6 Hz) and visual stimuli (1.8 Hz) in 5-second-long time windows (Figs. 2b and 3a). This yielded 8 (auditory) and 9 (visual) stimulus onsets and thus phase values per window. The choice for the length of the window for moving ITC and moving alpha amplitude analyses was the result of trying to achieve a balance between number of trials for ITC measure (greater number gives a better estimate), and keeping it shorter than the average inter-target interval (6 s), so that we could capture task structure related fluctuations in entrainment. To achieve a relatively good frequency resolution, in the <0.2 Hz frequency range we decided to use a 1 second stepping of the window, which resulted in a 4 s overlap. Using the Rayleigh statistic, we determined whether the ITC value for a given 5-second-long window was significant or not. This enabled us to sort trials into 4 different entrainment based categories: 1) significant delta ITC related to auditory stimuli (ITCa), 2) significant delta ITC related to visual stimuli (ITCv), 3) lack of any significant ITC (noITC) or 4) ITC to both stimuli (ITC both). Since the latter category occurred very rarely (Fig. 3b), and not in all experiments, we did not analyze neuronal activity during these time windows. Moving alpha amplitudes were calculated in the same time-windows, and were averaged across all cortical layers (Fig. 4a).

Given the lack of evoked responses to non-BF auditory and visual stimuli that could result in spurious phase bias, if delta ITC is significant in any given 5 second window, this indicates that delta oscillations in that period were well aligned to the timing of stimuli (Fig. 2b). Because in theory, phase alignment can be incidental if the frequency of ongoing delta oscillation is similar to the repetition rate of stimuli, we also tested whether mean phases for significant ITC time-periods were biased. The rationale is that if phase alignment is incidental from time to time (resulting in occasional high ITC), this should yield a random mean phase distribution, while true entrainment should result in a biased phase distribution (i.e. similar mean phases for high ITC time periods). We found that the distributions of mean phases for significant ITC periods were significantly biased in all recordings analyzed (Rayleigh test, all $p<0.05$), for both the auditory and visual stimulus streams, indicating that significant ITC values indeed index oscillatory entrainment.

To compensate for the varying numbers of trials across entrainment categories potentially biasing ITC measures[58], we used a repetitive combination technique to calculate ITC: for each group of trials in each experiment, we randomly drew 50 from all available trials, calculated ITC, repeated this 100 times, and averaged the 100 ITC values (Fig. 3c). Burst-CSD and spike-CSD coherence values were calculated the same way. This allowed us to statistically compare delta-theta vs. alpha-beta spike-CSD coherence between the groups of 100 ITC spectra for entrainment vs. 100 ITC spectra for no entrainment time periods for each single unit individually (Wilcoxon signed rank, $p<0.01$; Fig. 6d.).

Laminar oscillatory amplitudes across different recordings were aligned by interpolating amplitude values across channels from the electrode on the top of the cortex to the electrode on the bottom of the cortex to a constant 500 data points. This allowed us to statistically compare layer specific amplitude changes between different entrainment conditions across all A1 recordings (Fig. 3d).

Gamma bursts were identified by first using a publicly available Matlab peak detection algorithm (peakfinder by Nathanael C. Yoder, matlab central), with default settings. Next we selected bursts that had a clear peak in not just time, but also in the gamma frequency range (30 – 55). This was done by omitting bursts which had their largest energy around the "edges" of the gamma band (either at 30 or 55 Hz), to avoid wide band, usually 1/f spectral composition artifacts that would also create a gamma peak in the time domain.

Single unit isolation and sorting was performed offline using the Plexon Offline Sorter. To avoid classifying the same units as different in attend auditory vs. attend visual trial blocks of the same experiment due to possible electrode movement between the times when the two blocks were recorded, we only utilized attend auditory trial blocks for single unit analyses. Spike detection threshold was set manually to 3.5 standard deviation of the 300–5000Hz bandpass filtered signal. Spikes were sorted using the *K*-means algorithm, and only neurons with a downward voltage deflection followed by an upward peak were included in the analyses (Fig. 6a).

Delta and alpha coherence between all electrode pairs that yielded the laminar coherence matrices in Figure 7 were calculated at 1.6 Hz and 11 Hz using standard techniques in 5-second-long sliding windows, similar to moving delta ITC. This allowed us to test changes in cross-laminar coherence during periods of entrainment vs. no entrainment within each recording (Fig 7a).

## Statistics

Statistical analyses were performed in Matlab. We used either two-sided non-parametric Wilcoxon rank sum tests or Wilcoxon signed rank tests to compare two groups of values. To determine whether a group of values was significantly different from 0, we used a two-sided t-test (Fig. 7b). For multiple groups, we used either a two-way ANOVA or a Kruskal-Wallis test followed by the multiple comparison test (multcompare), using Tukey's honest significant criterion (Tukey's test). Data distribution was assumed to be normal but this was not formally tested. Significant deviation from uniform (random) phase distribution was tested with Rayleigh's uniformity test. No statistical methods were used to pre-determine

sample sizes; the number of animals was minimized to conform to ethical guidelines while keeping sample sizes similar to those reported in previous publications[6–8,14,24,25,30,45,59,60]. No animals or data points were excluded from the analyses.

### Data availability

The data that support the findings of this study are available from the corresponding author upon request

A Supplementary M**ethods** C**hecklist** is available.

## Supplementary Material

Refer to Web version on PubMed Central for supplementary material.

## Acknowledgments

Support for this work was provided by NIH grant R01DC012947 from the NIDCD (P.L.) and R01MH109289 from the NIMH (D.C.J.).

## References

1. Buzsáki, G. Rhythms of the brain. Oxford University Press; 2006.
2. Fries P. Rhythms for Cognition: Communication through Coherence. Neuron. 2015; 88:220–235. DOI: 10.1016/j.neuron.2015.09.034 [PubMed: 26447583]
3. Gray CM, Konig P, Engel AK, Singer W. Oscillatory responses in cat visual cortex exhibit inter-columnar synchronization which reflects global stimulus properties. Nature. 1989; 338:334–337. DOI: 10.1038/338334a0 [PubMed: 2922061]
4. Dragoi G, Buzsaki G. Temporal encoding of place sequences by hippocampal cell assemblies. Neuron. 2006; 50:145–157. DOI: 10.1016/j.neuron.2006.02.023 [PubMed: 16600862]
5. O'Keefe J, Conway DH. Hippocampal place units in the freely moving rat: why they fire where they fire. Exp Brain Res. 1978; 31:573–590. [PubMed: 658182]
6. Buschman TJ, Miller EK. Top-down versus bottom-up control of attention in the prefrontal and posterior parietal cortices. Science. 2007; 315:1860–1862. DOI: 10.1126/science.1138071 [PubMed: 17395832]
7. Lakatos P, Karmos G, Mehta AD, Ulbert I, Schroeder CE. Entrainment of neuronal oscillations as a mechanism of attentional selection. Science. 2008; 320:110–113. DOI: 10.1126/science.1154735 [PubMed: 18388295]
8. Womelsdorf T, Fries P, Mitra PP, Desimone R. Gamma-band synchronization in visual cortex predicts speed of change detection. Nature. 2006; 439:733–736. DOI: 10.1038/nature04258 [PubMed: 16372022]
9. Biswal B, Yetkin FZ, Haughton VM, Hyde JS. Functional connectivity in the motor cortex of resting human brain using echo-planar MRI. Magn Reson Med. 1995; 34:537–541. [PubMed: 8524021]
10. Fox MD, et al. The human brain is intrinsically organized into dynamic, anticorrelated functional networks. Proc Natl Acad Sci U S A. 2005; 102:9673–9678. DOI: 10.1073/pnas.0504136102 [PubMed: 15976020]
11. Weissman DH, Roberts KC, Visscher KM, Woldorff MG. The neural bases of momentary lapses in attention. Nat Neurosci. 2006; 9:971–978. DOI: 10.1038/nn1727 [PubMed: 16767087]
12. Allers KA, et al. Multisecond periodicities in basal ganglia firing rates correlate with theta bursts in transcortical and hippocampal EEG. J Neurophysiol. 2002; 87:1118–1122. [PubMed: 11826075]
13. de Pasquale F, et al. Temporal dynamics of spontaneous MEG activity in brain networks. Proc Natl Acad Sci U S A. 2010; 107:6040–6045. DOI: 10.1073/pnas.0913863107 [PubMed: 20304792]

14. Leopold DA, Murayama Y, Logothetis NK. Very slow activity fluctuations in monkey visual cortex: implications for functional brain imaging. Cereb Cortex. 2003; 13:422–433. [PubMed: 12631571]
15. Werner G, Mountcastle VB. The Variability of Central Neural Activity in a Sensory System, and Its Implications for the Central Reflection of Sensory Events. J Neurophysiol. 1963; 26:958–977. [PubMed: 14084169]
16. Castellanos FX, et al. Varieties of attention-deficit/hyperactivity disorder-related intra-individual variability. Biol Psychiatry. 2005; 57:1416–1423. DOI: 10.1016/j.biopsych.2004.12.005 [PubMed: 15950016]
17. Leth-Steensen C, Elbaz ZK, Douglas VI. Mean response times, variability, and skew in the responding of ADHD children: a response time distributional approach. Acta Psychol (Amst). 2000; 104:167–190. [PubMed: 10900704]
18. Smit DJ, Linkenkaer-Hansen K, de Geus EJ. Long-range temporal correlations in resting-state alpha oscillations predict human timing-error dynamics. J Neurosci. 2013; 33:11212–11220. DOI: 10.1523/JNEUROSCI.2816-12.2013 [PubMed: 23825424]
19. Ding N, Simon JZ. Emergence of neural encoding of auditory objects while listening to competing speakers. Proc Natl Acad Sci U S A. 2012; 109:11854–11859. DOI: 10.1073/pnas.1205381109 [PubMed: 22753470]
20. Lakatos P, et al. The spectrotemporal filter mechanism of auditory selective attention. Neuron. 2013; 77:750–761. DOI: 10.1016/j.neuron.2012.11.034 [PubMed: 23439126]
21. Zion Golumbic EM, et al. Mechanisms underlying selective neuronal tracking of attended speech at a “cocktail party”. Neuron. 2013; 77:980–991. DOI: 10.1016/j.neuron.2012.12.037 [PubMed: 23473326]
22. Freeman JA, Nicholson C. Experimental optimization of current source-density technique for anuran cerebellum. J Neurophysiol. 1975; 38:369–382. [PubMed: 165272]
23. O’Connell MN, Barczak A, Schroeder CE, Lakatos P. Layer specific sharpening of frequency tuning by selective attention in primary auditory cortex. J Neurosci. 2014; 34:16496–16508. DOI: 10.1523/JNEUROSCI.2055-14.2014 [PubMed: 25471586]
24. O’Connell MN, Falchier A, McGinnis T, Schroeder CE, Lakatos P. Dual mechanism of neuronal ensemble inhibition in primary auditory cortex. Neuron. 2011; 69:805–817. DOI: 10.1016/j.neuron.2011.01.012 [PubMed: 21338888]
25. Bastos AM, et al. Visual areas exert feedforward and feedback influences through distinct frequency channels. Neuron. 2015; 85:390–401. DOI: 10.1016/j.neuron.2014.12.018 [PubMed: 25556836]
26. Buffalo EA, Fries P, Landman R, Liang H, Desimone R. A backward progression of attentional effects in the ventral stream. Proc Natl Acad Sci U S A. 2010; 107:361–365. DOI: 10.1073/pnas.0907658106 [PubMed: 20007766]
27. Jensen O, Bonnefond M. Prefrontal alpha- and beta-band oscillations are involved in rule selection. Trends Cogn Sci. 2013; 17:10–12. DOI: 10.1016/j.tics.2012.11.002 [PubMed: 23176827]
28. Michalareas G, et al. Alpha-Beta and Gamma Rhythms Subserve Feedback and Feedforward Influences among Human Visual Cortical Areas. Neuron. 2016
29. Bonnefond M, Jensen O. Gamma activity coupled to alpha phase as a mechanism for top-down controlled gating. PLoS One. 2015; 10:e0128667. [PubMed: 26039691]
30. Spaak E, Bonnefond M, Maier A, Leopold DA, Jensen O. Layer-specific entrainment of gamma-band neural activity by the alpha rhythm in monkey visual cortex. Curr Biol. 2012; 22:2313–2318. DOI: 10.1016/j.cub.2012.10.020 [PubMed: 23159599]
31. van Kerkoerle T, et al. Alpha and gamma oscillations characterize feedback and feedforward processing in monkey visual cortex. Proc Natl Acad Sci U S A. 2014; 111:14332–14341. DOI: 10.1073/pnas.1402773111 [PubMed: 25205811]
32. Csicsvari J, Hirase H, Czurko A, Mamiya A, Buzsaki G. Oscillatory coupling of hippocampal pyramidal cells and interneurons in the behaving Rat. J Neurosci. 1999; 19:274–287. [PubMed: 9870957]

33. McCormick DA, Connors BW, Lighthall JW, Prince DA. Comparative electrophysiology of pyramidal and sparsely spiny stellate neurons of the neocortex. J Neurophysiol. 1985; 54:782–806. [PubMed: 2999347]
34. Nowak LG, Azouz R, Sanchez-Vives MV, Gray CM, McCormick DA. Electrophysiological classes of cat primary visual cortical neurons in vivo as revealed by quantitative analyses. J Neurophysiol. 2003; 89:1541–1566. DOI: 10.1152/jn.00580.2002 [PubMed: 12626627]
35. Robbins AA, Fox SE, Holmes GL, Scott RC, Barry JM. Short duration waveforms recorded extracellularly from freely moving rats are representative of axonal activity. Front Neural Circuits. 2013; 7:181. [PubMed: 24348338]
36. Laufs H, et al. Electroencephalographic signatures of attentional and cognitive default modes in spontaneous brain activity fluctuations at rest. Proc Natl Acad Sci U S A. 2003; 100:11053–11058. DOI: 10.1073/pnas.1831638100 [PubMed: 12958209]
37. Mantini D, Perrucci MG, Del Gratta C, Romani GL, Corbetta M. Electrophysiological signatures of resting state networks in the human brain. Proc Natl Acad Sci U S A. 2007; 104:13170–13175. DOI: 10.1073/pnas.0700668104 [PubMed: 17670949]
38. Murphy K, Birn RM, Handwerker DA, Jones TB, Bandettini PA. The impact of global signal regression on resting state correlations: are anti-correlated networks introduced? Neuroimage. 2009; 44:893–905. DOI: 10.1016/j.neuroimage.2008.09.036 [PubMed: 18976716]
39. van den Brink RL, Wynn SC, Nieuwenhuis S. Post-error slowing as a consequence of disturbed low-frequency oscillatory phase entrainment. J Neurosci. 2014; 34:11096–11105. DOI: 10.1523/JNEUROSCI.4991-13.2014 [PubMed: 25122906]
40. Haegens S, Nacher V, Luna R, Romo R, Jensen O. alpha-Oscillations in the monkey sensorimotor network influence discrimination performance by rhythmical inhibition of neuronal spiking. Proc Natl Acad Sci U S A. 2011; 108:19377–19382. DOI: 10.1073/pnas.1117190108 [PubMed: 22084106]
41. Foxe JJ, Snyder AC. The Role of Alpha-Band Brain Oscillations as a Sensory Suppression Mechanism during Selective Attention. Front Psychol. 2011; 2:154. [PubMed: 21779269]
42. Saalmann YB, Pinsk MA, Wang L, Li X, Kastner S. The pulvinar regulates information transmission between cortical areas based on attention demands. Science. 2012; 337:753–756. DOI: 10.1126/science.1223082 [PubMed: 22879517]
43. Womelsdorf T, Valiante TA, Sahin NT, Miller KJ, Tiesinga P. Dynamic circuit motifs underlying rhythmic gain control, gating and integration. Nat Neurosci. 2014; 17:1031–1039. DOI: 10.1038/nn.3764 [PubMed: 25065440]
44. Hutcheon B, Yarom Y. Resonance, oscillation and the intrinsic frequency preferences of neurons. Trends Neurosci. 2000; 23:216–222. [PubMed: 10782127]
45. Lakatos P, Schroeder CE, Leitman DI, Javitt DC. Predictive suppression of cortical excitability and its deficit in schizophrenia. J Neurosci. 2013; 33:11692–11702. DOI: 10.1523/JNEUROSCI.0010-13.2013 [PubMed: 23843536]
46. Garrity AG, et al. Aberrant “default mode” functional connectivity in schizophrenia. Am J Psychiatry. 2007; 164:450–457. DOI: 10.1176/ajp.2007.164.3.450 [PubMed: 17329470]
47. Whitfield-Gabrieli S, et al. Hyperactivity and hyperconnectivity of the default network in schizophrenia and in first-degree relatives of persons with schizophrenia. Proc Natl Acad Sci U S A. 2009; 106:1279–1284. DOI: 10.1073/pnas.0809141106 [PubMed: 19164577]
48. Kim JS, et al. Power spectral aspects of the default mode network in schizophrenia: an MEG study. BMC Neurosci. 2014; 15:104. [PubMed: 25189680]
49. Lakatos P, O’Connell MN, Barczak A. Pondering the Pulvinar. Neuron. 2016; 89:5–7. DOI: 10.1016/j.neuron.2015.12.022 [PubMed: 26748085]
50. Calderone DJ, Lakatos P, Butler PD, Castellanos FX. Entrainment of neural oscillations as a modifiable substrate of attention. Trends Cogn Sci. 2014; 18:300–309. DOI: 10.1016/j.tics.2014.02.005 [PubMed: 24630166]
51. Legatt AD, Arezzo J, Vaughan HG Jr. Averaged multiple unit activity as an estimate of phasic changes in local neuronal activity: effects of volume-conducted potentials. J Neurosci Methods. 1980; 2:203–217. [PubMed: 6771471]

52. Mitzdorf U. Current source-density method and application in cat cerebral cortex: investigation of evoked potentials and EEG phenomena. Physiol Rev. 1985; 65:37–100. [PubMed: 3880898]

53. Lakatos P, et al. Timing of pure tone and noise-evoked responses in macaque auditory cortex. Neuroreport. 2005; 16:933–937. [PubMed: 15931064]

54. Steinschneider M, Reser D, Schroeder CE, Arezzo JC. Tonotopic organization of responses reflecting stop consonant place of articulation in primary auditory cortex (A1) of the monkey. Brain Res. 1995; 674:147–152. [PubMed: 7773684]

55. Slotnick B. A simple 2-transistor touch or lick detector circuit. J Exp Anal Behav. 2009; 91:253–255. DOI: 10.1901/jeab.2009.91-253 [PubMed: 19794837]

56. Merzenich MM, Brugge JF. Representation of the cochlear partition of the superior temporal plane of the macaque monkey. Brain Res. 1973; 50:275–296. [PubMed: 4196192]

57. Rauschecker JP, Tian B, Pons T, Mishkin M. Serial and parallel processing in rhesus monkey auditory cortex. J Comp Neurol. 1997; 382:89–103. [PubMed: 9136813]

58. Maris E, Schoffelen JM, Fries P. Nonparametric statistical testing of coherence differences. J Neurosci Methods. 2007; 163:161–175. DOI: 10.1016/j.jneumeth.2007.02.011 [PubMed: 17395267]

59. Kajikawa, Y.; Falchier, A.; Musacchia, G.; Lakatos, P.; Schroeder, CE. The Neural Bases of Multisensory Processes Frontiers in Neuroscience. Murray, MM.; Wallace, MT., editors. 2012.

60. Schroeder CE, Molhom S, Lakatos P, Ritter W, Foxe JJ. Human–simian correspondence in the early cortical processing of multisensory cues. Cognitive Processing. 2004; 5:140–151.

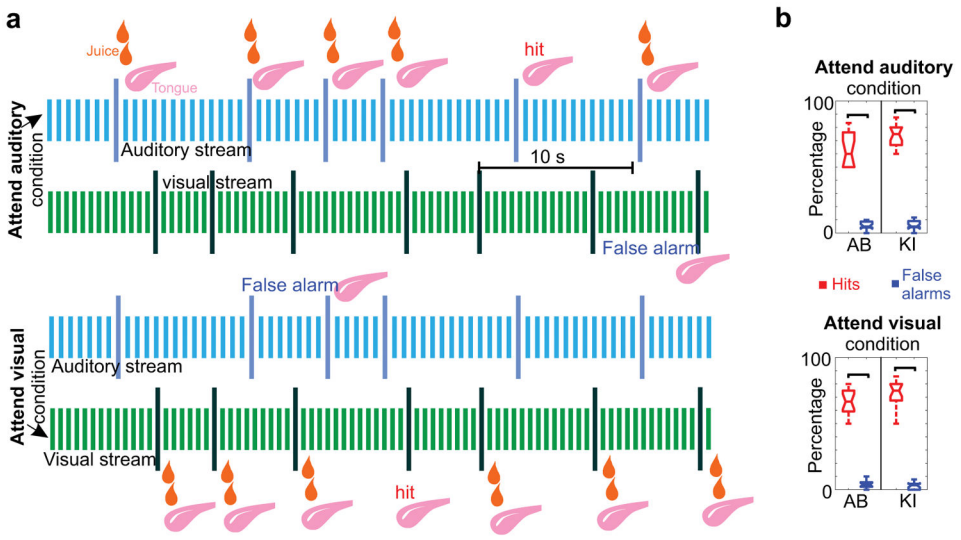


**Figure 1. Intermodal selective attention paradigm**

(**a**) All data presented were recorded while subjects were performing an intermodal selective attention task: they were cued to either detect deviant stimuli in the auditory (attend auditory) or the visual (attend visual) simultaneously presented stimulus sequences (streams). Visual and auditory stimuli were identical in the two different cue contexts. On 80% of the deviants of the cued modality, a juice reward was presented and subjects had to stick out their tongue in order to get it. Performance was monitored by detecting licking on juiceless deviants (hit). If subjects were licking following a deviant in the un-cued, to be ignored modality, we considered this a false alarm. (**b**) Both subjects' hit rates were significantly higher than their false alarm rates across experiments ($n_{AB}$=16, $p_{auditory}$=4.37×10$^{-04}$, $p_{visual}$=4.37×10$^{-04}$ for subject AB and $n_{KI}$=20, $p_{auditory}$=8.83×10$^{-05}$, $p_{visual}$=8.82×10$^{-05}$ for subject KI,, Wilcoxon signed rank). One of the subjects (KI) had a significantly higher hit rate (76% vs. 64%) than the other across both attend auditory and attend visual trial blocks (($n_{AB}$ = 16, $n_{KI}$ = 20, Wilcoxon rank sum, $p_{auditory}$=0.03, $p_{visual}$=0.02)). Mean false alarm rates were around 5% for both subjects, and did not differ significantly ($n_{AB}$ = 16, $n_{KI}$ = 20, Wilcoxon rank sum, $p_{auditory}$=0.42, $p_{visual}$=0.49). Boxplots have lines at lower quartile, median, and upper quartile values, while whiskers show the extent of the data.

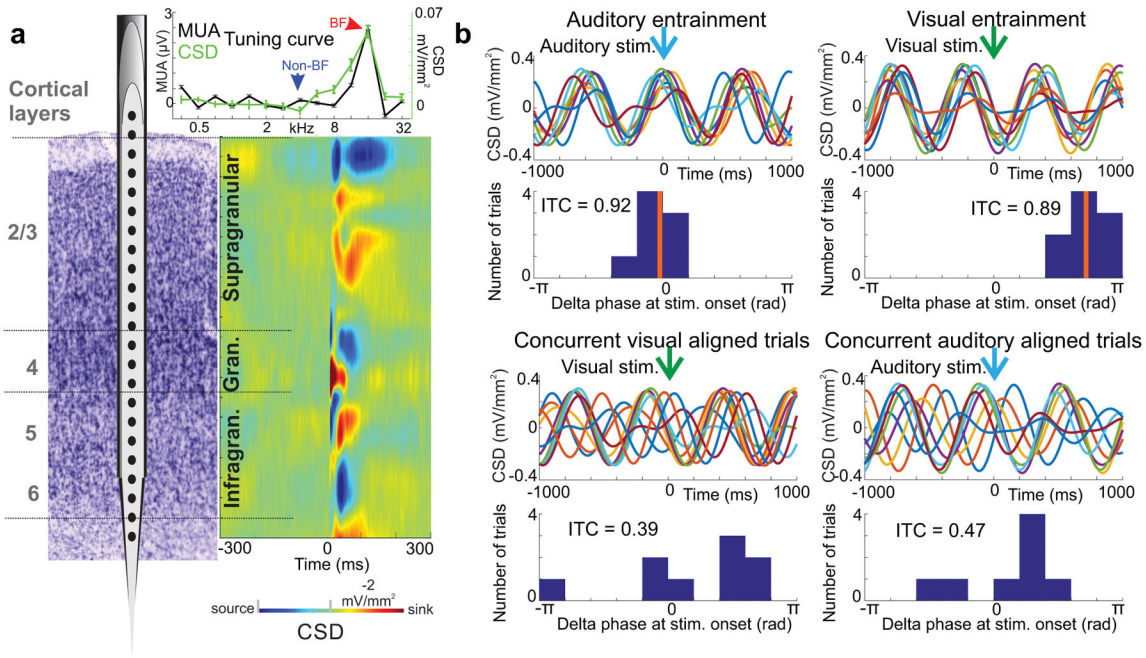


**Figure 2. Recording technique and inter-trial coherence (ITC)**

(**a**) To the right of the schematic of the linear array multicontact electrode positioned in primary auditory cortex, the colormap shows a characteristic BF tone related laminar CSD response profile. Current sinks (net inward transmembrane current) are red and current sources (net outward transmembrane current) are blue. Laminar boundaries (horizontal lines) were determined based on functional criteria. The inset above is the tuning curve for the representative A1 site derived from MUA (black) and CSD (green) response amplitudes to a range of different frequency pure tones. The arrows denote the BF and a frequency 2 octaves away, designated as non-BF. **(b)** An illustration of how our ITC measure, with a value range of 0 to 1, indexes the phase alignment to stimuli in a given sensory stream. All traces in this figure panel show single trials of supragranular CSD, filtered in the delta frequency band (1– 2.5 Hz). To the left, traces on the top depict 8 single trials aligned to the timing of auditory stimuli, occurring within a 5 second time window. In this particular window, delta phases at stimulus onset are heavily biased (clustered in the histogram), resulting in significant delta ITC (Rayleigh test, n = 8, $p= 6.59\times10^{-06}$), and indicating entrainment. The panel below shows 9 single trials during the same 5 second period, but aligned to visual stimulus onset. The histogram in this case signifies a random delta phase distribution with non-significant ITC (Rayleigh test, n= 9, p = 0.24). To the right, both the single trial traces and the delta phase distribution resulting in significant ITC (Rayleigh test, n = 9, $p=2.5\times10^{-05}$) indicate entrainment to visual stimuli. In contrast, delta band neuronal activity in the same time window is not aligned to the timing of auditory stimuli that form the simultaneously presented auditory stream, resulting in non-significant ITC (Rayleigh test, n = 8, p=0.49).

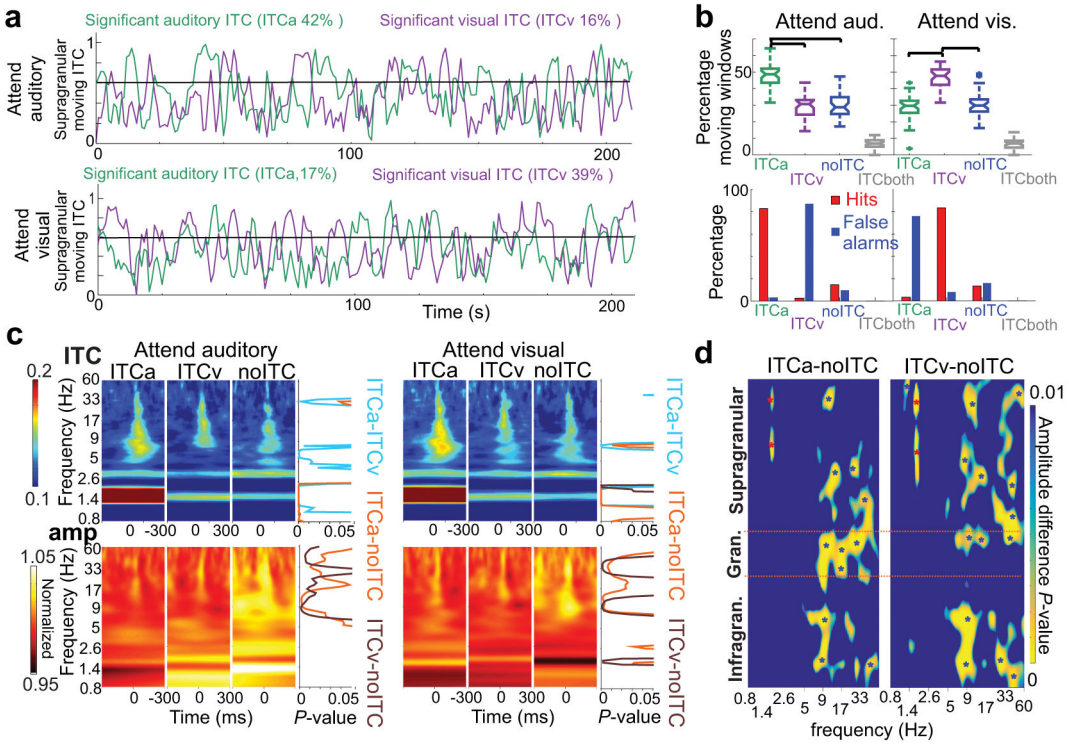


**Figure 3. Long timescale dynamics of oscillatory entrainment during a continuous selective intermodal attention task**

(**a**) Moving delta ITC values from a representative supragranular electrode site. Green traces were calculated using the timing of non-BF tones, while purple traces were calculated using the timing of LED flashes in attend auditory (top) and attend visual (bottom) trial blocks. The black horizontal line denotes the level above which auditory moving ITC is significant. (**b**) On top, green and purple boxplots show the percentage of time windows with significant auditory (ITCa), and visual (ITCv) delta ITC respectively, during attend auditory (left) vs. attend visual (right) trial blocks across all experiments (n=36). Blue and gray boxplots show the percentage of time windows with no significant delta ITC related to any of the streams (noITC), and significant ITC related to both streams (ITCboth). Boxplots have lines at lower quartile, median, and upper quartile values, while whiskers show the extent of the data. Significant ITC indicating entrainment occurred significantly more related to cued modality streams (n=36, Tukey's test, attend auditory: $p_{ITCa\text{-}ITCv}=2.33\times10^{-6}$, $p_{ITCa\text{-}noITC}=3.67\times10^{-6}$, $p_{ITCa\text{-}ITCboth}=3.77\times10^{-9}$, $p_{ITCv\text{-}noITC}=0.99$, $p_{ITCv\text{-}ITCboth}=1.3\times10^{-7}$, $p_{noITC\text{-}ITCboth}=7.9\times10^{-8}$; attend visual: $p_{ITCa\text{-}ITCv}=1.51\times10^{-6}$, $p_{ITCa\text{-}noITC}=0.97$, $p_{ITCa\text{-}ITCboth}=5.18\times10^{-7}$, $p_{ITCv\text{-}noITC}=1.32\times10^{-5}$, $p_{ITCv\text{-}ITCboth}=3.77\times10^{-9}$, $p_{noITC\text{-}ITCboth}=4.89\times10^{-8}$). On the bottom, bars denote the percentage of hits and false alarms during the same 4 time periods demarcated by differing ITC (ITCa, ITCv, noITC and ITCboth). Hits during periods of no entrainment (noITC) occurred significantly less than during entrainment by the cued modality stimuli (n=36, Wilcoxon signed rank, $p_{attend\_auditory}=1.8\times10^{-7}$, $p_{attend\_visual}=1.4\times10^{-7}$), and false alarms occurred significantly less than during entrainment by the to be ignored modality stimuli ($p_{attend\_auditory}=7.8\times10^{-4}$, $p_{attend\_visual}=3.5\times10^{-6}$). (**c**) Auditory non-BF stimulus related ITC (upper) and amplitude

(lower) time-frequency plots averaged across attend auditory (left) and attend visual (right) trial blocks during ITCa, ITCv, and noITC time-periods. To the right of the plots, traces show frequency specific p values (Wilcoxon signed rank, corrected) derived from statistically comparing ITC and amplitude values amongst ITCa-ITCv (light blue), ITCa-noITC (gold) and ITCv-noITC (brown) time-periods. (**d**) Laminar profiles of frequency (x axis) specific, Bonferroni corrected p values derived from statistically comparing amplitudes between ITCa-noITC and ITCv-noITC time-periods across all experiments (n=36) and cueing conditions (n=36*2=72, Wilcoxon signed rank). The blue color represents p values above 0.01. Red stars on the color-maps denote p values below 0.001 indicating significantly larger amplitudes in ITCa or ITCv vs. noITC conditions, while blue stars indicate significantly larger amplitudes during noITC time periods.

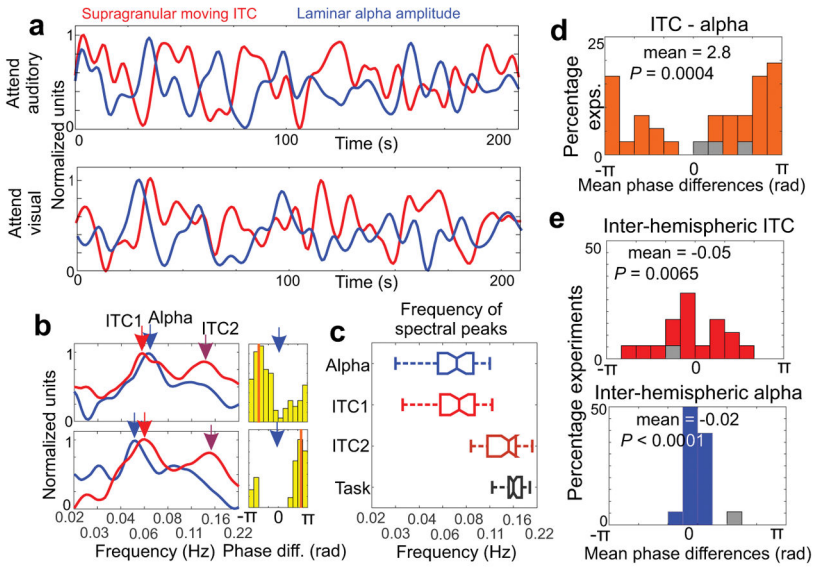


**Figure 4. Slow counterphase fluctuation of delta oscillatory entrainment and alpha amplitude**

(**a**) Low pass filtered supragranular moving ITC and cross-laminar alpha amplitude waveforms from a representative attend auditory (top) and attend visual (bottom) trial block (same blocks as in Fig. 3a). (**b**) Representative spectra of supragranular moving ITC and cross-laminar alpha amplitude from 2 experiments. Light and dark red arrows denote prominent peaks in the spectrum of moving ITC, while blue arrows denote prominent peaks in the spectrum of moving alpha amplitude signals. Histograms to the right display the distribution of ITC-alpha phase difference at the frequency of the alpha spectrogram peak throughout the trial blocks. (**c**) Boxplots show the frequency of moving alpha (blue) and moving ITC spectral peaks (light red for the lower and dark red for the higher frequency peak), and the task frequency (grey) from all trial blocks. The boxplots have lines at lower quartile, median, and upper quartile values, while whiskers show the extent of the data. (**d**) Histogram shows that ITC-alpha mean phase differences pooled across experiments are significantly biased (n=36, Rayleigh test, p value and mean phase are displayed in the figure). Grey color denotes mean phases of non-significantly biased phase distributions. (**e**) The distributions of ITC-ITC (top) and alpha-alpha (bottom) mean phase differences derived from concurrently recorded left and right hemisphere A1 neuronal ensemble activity indicate synchronous modulation across hemispheres (n=18, Rayleigh test, p values and mean phases are displayed in the figure).

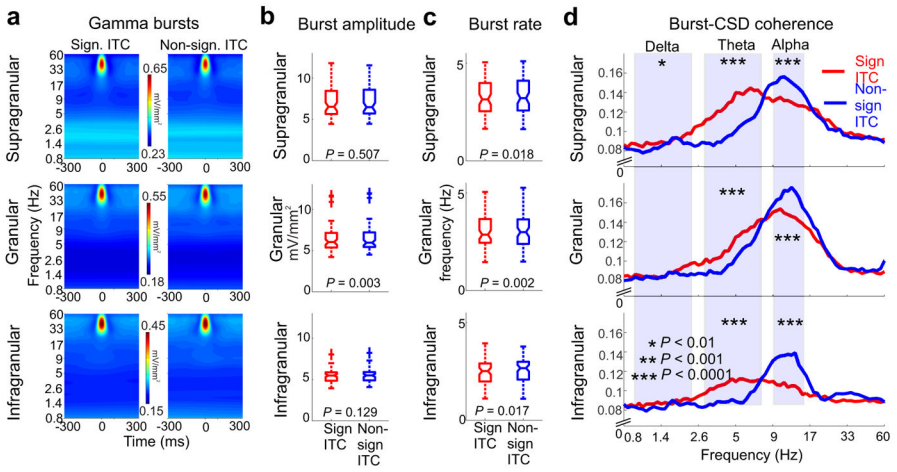


**Figure 5. Entrainment correlated patterns of cross-frequency coupling**

(**a**) Time frequency amplitude maps show gamma bursts averaged across all experiments during time periods of entrainment (significant ITC, left) and no entrainment(non-significant ITC, right) from the different cortical layers. (**b**) Gamma burst amplitudes pooled across all experiments and cueing conditions during significant ITC (red) and non-significant ITC (blue) time-periods only show a significant difference in the granular layer (n=72, Wilcoxon signed rank, p values are displayed in the figure). The boxplots have lines at lower quartile, median, and upper quartile values, while whiskers show the extent of the data. (**c**) The rate of gamma bursts in different layers during significant ITC (red) and non-significant ITC (blue) time-periods shows a significant difference across all layers (n=72, Wilcoxon signed rank, p values are displayed in the figure)). As in panel B, the boxplots have lines at lower quartile, median, and upper quartile values, while whiskers show the extent of the data. (**d**) Layer specific burst-CSD coherence spectra. Stars denote significant differences in the delta, theta, and alpha frequency ranges in significant ITC vs. non-significant ITC periods (n=72, Wilcoxon signed rank, supragranular: $p_{delta}=0.0014$, $p_{theta}=8.1\times10^{-12}$, $p_{alpha}=5.5\times10^{-5;}$ granular: $p_{delta}=0.03$, $p_{theta}=1.5\times10^{-5}$, $p_{alpha}=2.6\times10^{-5;}$ infragranular: $p_{delta}=0.09$, $p_{theta}=2.9\times10^{-5}$, $p_{alpha}=2\times10^{-6}$).

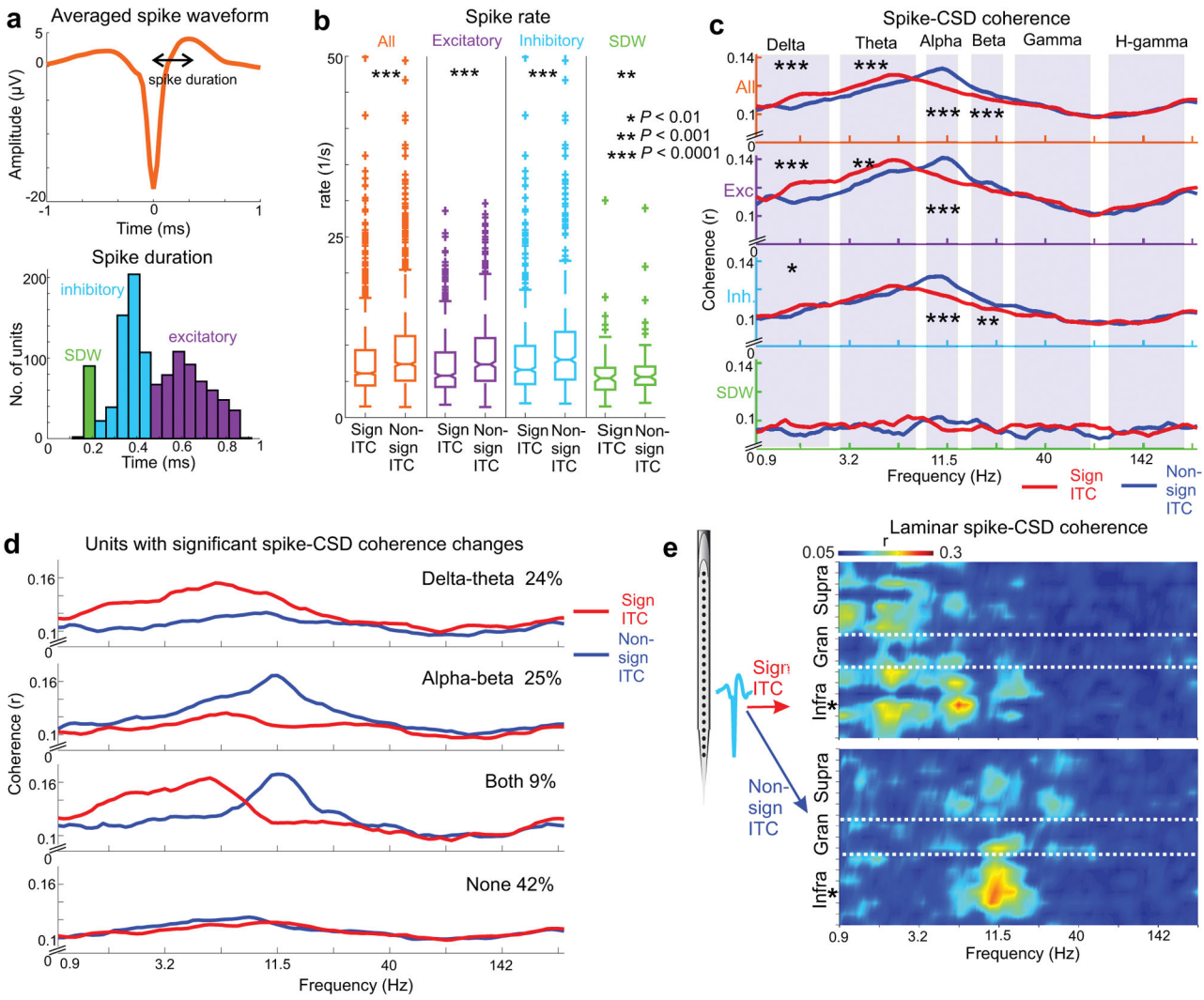


**Figure 6. Distinct brain state dependent patterns of single unit activity**

(**a**) Spike waveform averaged across all single units (n=1167). Spike duration was measured as the time between the negative peak used to detect and align spikes, and the subsequent positive peak. Histogram below displays the distribution of spike durations. Putatively, short, medium, and long spike durations represent afferent spikes (SDW), and the firing of inhibitory and excitatory neurons respectively. (**b**) Pooled spike rates of all neurons (orange) and the different unit types during significant ITC and non-significant ITC time-periods. Stars denote significant firing rate increases during non-significant ITC periods ($n_{all}$=1167, $n_{inhibitory}$=589, $n_{excitatory}$=490, $n_{SDW}$=88, Wilcoxon signed rank, $p_{all}=2.5\times10^{-123}$, $p_{excitatory}=4.9\times10^{-55}$, $p_{inhibitory}=5.5\times10^{-65}$, $p_{SDW}=8.1\ x10^{-4}$). The boxplots have lines at lower quartile, median, and upper quartile values, while whiskers show the extent of the data. (**c**) Unit specific spike-CSD coherence spectra during significant ITC (red) vs. non-significant ITC (blue) periods. Stars denote significant differences in the frequency ranges marked by shaded regions ($n_{all}$=1167, $n_{inhibitory}$=589, $n_{excitatory}$=490, $n_{SDW}$=88, Wilcoxon signed rank, all: $p_{delta}=1.5\times10^{-6}$, $p_{theta}=3.3\times10^{-5}$, $p_{alpha}=2.4\times10^{-20}$, $p_{beta}=9.2\times10^{-5}$,

$p_{gamma}$=0.72, $p_{hgamma}$=0.08; excitatory: $p_{delta}=8.3\times10^{-6}$, $p_{theta}=9.3\times10^{-4}$, $p_{alpha}=1.1\times10^{-7}$, $p_{beta}$=0.055, $p_{gamma}$=0.33, $p_{hgamma}$=0.0197; inhibitory: $p_{delta}$=0.002, $p_{theta}$=0.015, $p_{alpha}=1.9\times10^{-13}$, $p_{beta}=6.1\times10^{-4}$, $p_{gamma}$=0.062, $p_{hgamma}$=0.75; SDW: $p_{delta}$=0.45, $p_{theta}$=0.27, $p_{alpha}$=0.02, $p_{beta}$=0.27, $p_{gamma}$=0.28, $p_{hgamma}$=0.71). (**d**) Top traces depict averaged spike-CSD coherence spectra of units with a significant delta-theta band spike-CSD coherence increase during significant ITC periods. Below, spike-CSD coherence spectra of units with a significant alpha-beta spike-CSD coherence decrease during the same periods. Further below, spike-CSD coherence spectra of units that display entrainment correlated coherence changes in both frequency bands, and lastly units that show no significant coherence change. (**e**) Laminar spike-CSD coherence spectra of a putative inhibitory neuron from the infragranular layers (location marked by the star) during significant ITC (top) and non-significant ITC (bottom) time periods.

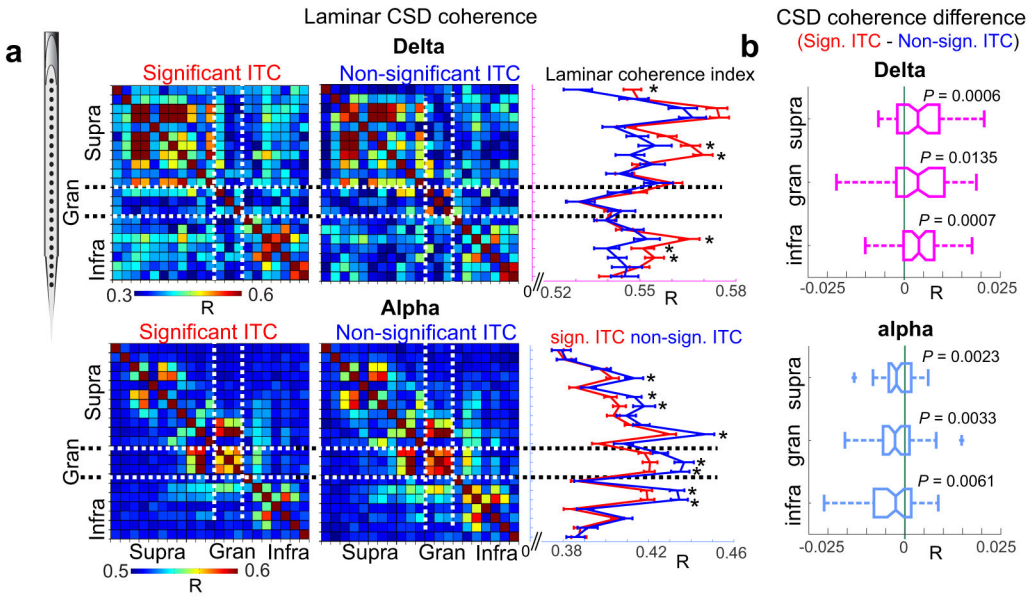


**Figure 7. Entrainment correlated changes in laminar delta and alpha coherence**

(**a**) Laminar delta (top) and alpha (bottom) coherence matrices calculated during significant ITC (left) and non-significant ITC (right) time periods. Traces to the right show coherence values (R) averaged along one dimension, error bars depict mean +/− standard error. Stars denote significant differences between significant ITC (red) and no-ITC (blue) periods ($n_{sig\text{-}ITC}$=137, $n_{no\text{-}ITC}$=61, Wilcoxon rank sum, p<0.01). (**b**) Layer specific difference of delta (magenta) and alpha (light blue) coherence (R) between significant ITC and non-significant ITC periods. The boxplots have lines at lower quartile, median, and upper quartile values, while whiskers show the extent of the data. The p values denote statistical significance for each distribution's difference from 0, which would indicate no change (n=72, one sample t-test, df=71, $t_{delta\text{-}supragranular}$=4.49, $t_{delta\text{-}granular}$=3.18, $t_{delta\text{-}infragranular}$=3.91, $t_{alpha\text{-}supragranular}$=−3.25, $t_{alpha\text{-}granular}$=−3.97, $t_{alpha\text{-}infragranular}$=−2.71, p-values are displayed in the figure label).